PERGAMON

International Journal of Solids and Structures 39 (2002) 1059–1075

INTERNATIONAL JOURNAL OF SOLIDS and STRUCTURES

www.elsevier.com/locate/ijsolstr

Modeling of the metal powder compaction process using the cap model. Part I. Experimental material characterization and validation

Hédi Chtourou [a,b,c], Michel Guillot [a,c], Augustin Gakwaya [a,c,*]

[a] *P/M Laboratory-Précitech Inc. and Université Laval, Quebec, Canada G1P 4P4*
[b] *Department of Technology, IPEIS, Sfax University, Tunisia*
[c] *Department of Mechanical Engineering, Laval University, Pavillon Pouliot, Sainte Foy, Quebec, Canada G1K 7P4*

Received 23 May 1997

Abstract

In order to produce crack free metal powder compacts that respect both the dimensional tolerances and the mechanical strength requirements, both tooling design and compaction sequence have to be adequately determined. The finite element method, through the use of an appropriate constitutive model of the powder medium, has recently been used as an efficient design tool. The accuracy of this method highly depends on the faithfulness of the constitutive model and the quality of the material parameter set. Furthermore, in order for the simulation results to be reliable, they should be experimentally validated on real parts featuring density variations. Hence, the main concerns of this paper are the development of a standard calibration procedure for the cap material model as well as the development of a reliable technique for the experimental validation of the powder compaction simulation results.

The developed calibration procedure, applied for the case of 316L stainless steel powders, is based on a series of isostatic, triaxial and uniaxial compaction tests as well as resonant frequency tests. In addition, a sensitivity study was performed in order to determine the relative importance of each factor and basic simulations served to validate the parameter set extraction procedure.

On the other hand, a local density measurement technique was developed for the experimental validation of the model results. This technique is based on correlation with Vickers macro-hardness. Finally, an application featuring the compaction of a 316L stainless steel cylindrical component is presented to illustrate the predictive capabilities of the cap material model as well as the accuracy of the acquired material parameter set. © 2002 Published by Elsevier Science Ltd.

Keywords: Powder metallurgy; Finite element; Simulation; Constitutive model; Material behavior; Cap model; Calibration; Validation; Local density

* Corresponding author. Address: Department of Mechanical Engineering, Laval University, Pavillon Pouliot, Sainte Foy, Quebec, Canada G1K 7P4. Tel.: +1-418-656-5548; fax: +1-418-656-7415.
E-mail address: agakwaya@gmc.ulaval.ca (A. Gakwaya).

0020-7683/02/$ - see front matter © 2002 Published by Elsevier Science Ltd.
PII: S0020-7683(01)00255-4

1. Introduction

Manufacturing parts using P/M involves four major activities: powder and lubricant mixing, compacting, sintering and finally, post-sintering secondary operations. Due to the nature of the metal powders and to their interaction with the compaction tools, complex mechanical mechanisms take place during the forming process (Lenel, 1980). These mechanisms are mainly the combination of the finite elastic–plastic deformation, the internal friction of the powder medium and its frictional contact with the tooling components. These phenomena typically lead to undesirable non-uniform density distribution and even to cracks within the pressed parts.

In order to produce crack free compacts that respect both the dimensional tolerances and the mechanical strength requirements, both tooling design and compaction sequence have to be adequately determined (Lenel, 1980; German, 1984). P/M engineers have developed an extensive ''know-how'' that is very helpful in designing routine parts, but when dealing with more complicated designs, costly trial and error procedures tend to be used. Instead of using traditional trial and error design approach, the finite element (FE) simulation method has recently been used as an alternative design tool. This method, through the use of an appropriate constitutive model of the powder medium, permits the prediction of density and stress distributions in the pressed compact prior to the actual tooling design and manufacturing activity.

Although the FE method has proved to be an excellent design tool, it should be noted that the accuracy of simulation results highly depend on the faithfulness of the constitutive model and the quality of the material parameter set. It is in fact recognized that, compared to similar models, the cap material model is capable of representing very well all of the powder compaction stages. Nevertheless, due to the large number of its parameters, no standard calibration procedures have yet been established. This explain why, despite its solid theoretical background, this model is not as popular as other models easier to calibrate (Brown and Abou-Chedid, 1993).

Furthermore, in order for the simulation results to be reliable, they should be experimentally validated on real parts featuring density variations. However, since measuring the local density distributions of brittle green compacts is a very delicate operation, no accurate measuring technique has been yet established. Hence, the main concerns of this paper are the development of a standard calibration procedure for the cap model as well as the development of a reliable technique for the experimental validation of the powder compaction simulation results.

Accordingly, the next section presents a brief review of the most common models used for the simulation of metal powder compaction and a more detailed presentation of the cap material model, used in this study. Subsequently, we present the developed calibration procedure as applied for the case of 316L stainless steel powders. This is based on a series of isostatic, triaxial and uniaxial compaction tests aimed at characterizing the powder hardening law and yield surfaces. Also, resonant frequency tests aimed at the characterization of the elastic behavior of the powder medium at several densities have been used. In addition, we present the results of a sensitivity study intended to determine the relative importance of each factor, as well as the results of basic simulations intended to validate the parameter set extraction procedure.

We will then present a local density measurement technique used as the experimental validation method of the model results. This technique is based on correlation with Vickers macro-hardness. Finally, an application featuring the compaction of a 316L stainless steel cylindrical component is also presented to illustrate the predictive capabilities of the cap material model as well as the accuracy of the acquired material parameter set.

2. Powder material constitutive model

2.1. Basic modeling hypotheses

Modeling the compaction processes could be performed by two different approaches: the micro-mechanical and the macro-mechanical modeling. In the first approach, each particle is typically modeled as a sphere that interacts with surrounding particles (Jagota and Dawson, 1988a,b; Biba et al., 1993). The sphericity hypothesis is not applicable in cases where powders have dendritic or very irregular shapes. For this and other practical and computational reasons, the macro-mechanical modeling approach have been privileged in the literature. Thus, the powder medium is considered as a continuum that undergoes large elastic–plastic deformations. This is justified by the very small volume of a typical void compared to the volume of a typical compacted part. Furthermore, it is known that compacted powder remain globally isotropic even if small anisotropy is caused by compaction. Finally, it is widely assumed that the powder compaction process is inviscid and isothermal, especially when the speed of compaction tools is not very high (Crawford and Lindskog, 1983; Doraivelu et al., 1984; Kuhn and Downey, 1971; Shima and Oyane, 1976).

2.2. Material models in the literature

In the field of macro-mechanical modeling of the metal powder compaction, two types of models are generally used: the "classical elastoplasticity" models and the "soil mechanics" models. Models of the first group, also known as the "Kuhn–Shima" type of model were originally developed for sintered compacts and are simply an extension of the classical J_2-flow theory to the compressible range. This is done by introducing the first stress invariant into the yield criterion which takes then an ellipsoid shape in the spherical-deviatoric stress space (Fig. 1).

The general form of this kind of yield criteria is given in (Eq. (1)) where the parameters A, B and C are functions of the actual medium density ρ and where I_1 is the first invariant of the stress tensor, J_2 is the second invariant of the deviatoric stress tensor and k is a state variable representing the hardening effect.

$$f(\sigma,\rho,k) = A(\rho)I_1^2 + B(\rho)J_2 - C(\rho)k^2 \tag{1}$$

This type of model, based on the assumption that only powder particles undergo plastic deformation and that particle rearrangement is negligible, uses associative flow rule and isotropic hardening. It was originally proposed by Kuhn and Downey (1971) and the formulated differently by Shima and Oyane (1976), Weber and Brown (1989) and others (Doraivelu et al., 1984; Gurson and Posteraro, 1992). Recently, Brown and Abou-Chedid (1993) demonstrated that, due to shape of their yield surface and despite the fact that they

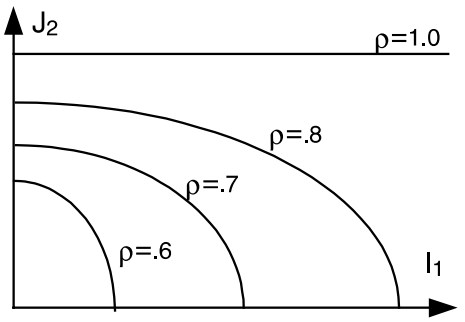

Fig. 1. Yield criterion of the Kuhn–Shima type of model.

correctly model the last stages of compaction, these models are not appropriate for modeling the early stages of compaction where the density level is very low. Following this observation, Koopman et al. (1992) and Shima and Saleh (1993) proposed significant changes to this model in order for it to better represent the shear behavior of the loose powder and to accommodate for internal friction.

On the other hand, the cap model is one of the most popular among the "soil mechanics" type of models. It was originally developed for rocks, soils and other geological materials (Dimaggio and Sandler, 1971; Sandler and Rubin, 1979). It is a multi-surface elastoplasticity model permitting the representation of densification, hardening as well as interparticle friction. Due to the similarities in behavioral response of geological materials and some hard metal powders, this model was adopted and used to simulate the cold die compaction of tungsten carbide powder (Crawford and Lindskog, 1983; Trasorras et al., 1989).

This kind of model was chosen in the present study because of the great flexibility it has shown in modeling all the compaction stages, especially the early ones. Provided some adjustments are performed (Trasorras et al., 1989; Chtourou et al., 1995), this model is suitable for the simulation of the compaction of ductile powders able to attain higher density ranges. However, a significant amount of experimental work is required in order to properly calibrate the model parameters for a particular blend of powders.

2.3. Formulation of the cap model

2.3.1. Stress–strain relationship

The adopted stress–strain relationship corresponds to that of an isotropic hyperelastic solid where the elasticity parameters are density dependent:

$$\sigma = \overline{\mathbf{C}}\varepsilon^{\mathrm{e}} = \overline{\mathbf{C}}(\varepsilon - \varepsilon^{\mathrm{p}}) \tag{2}$$

with

$$\overline{\mathbf{C}} = \frac{\partial^2 \psi}{\partial \varepsilon^2} = 2G(\rho)\overline{\mathbf{I}} + \left(K(\rho) - \frac{2G(\rho)}{3}\right)\mathbf{1} \otimes \mathbf{1} \tag{3}$$

In the equations above, ψ is an hyperelastic free energy, $\overline{\mathbf{C}}$ is the fourth order elasticity tensor, $\overline{\mathbf{I}}$ and $\mathbf{1}$ are respectively the fourth and second order identity tensors, G and K are the shear and bulk moduli expressed in terms of the powder relative density ρ.

2.3.2. Multi-yield surface and flow rule

Another main component of the constitutive model is the yield functions that separate the purely elastic behavior from the elastic–plastic one. For the cap model a multi-yield surface is usually adopted. Typically, when studying the behavior of compressible media, this function is formulated in terms of J_1, the stress first invariant and of s: the norm of the stress deviator $\mathbf{S}$ given by:

$$\mathbf{S} = \boldsymbol{\sigma} - \frac{J_1}{3}\mathbf{1} \tag{4}$$

In the J_1–s space, the elastic behavior region is bounded by three surfaces that intersect in a non-smooth manner (Fig. 2). These surfaces are respectively the tension and the shear failure surfaces and the strain hardening cap surface (Sandler and Rubin, 1979).

The tension and shear failure surfaces represent the limit stress states beyond which fracture of the powder compact may occur during its ejection or its compaction with very large local distortion. This is caused either by different compaction ratios of powder columns in multilevel parts or by the die wall friction. The two surfaces can respectively be represented by the following two functions (Trasorras et al., 1989; Hofstetter et al., 1993):

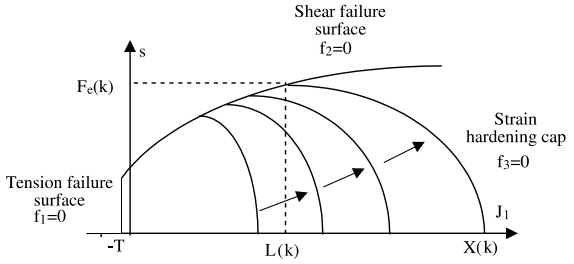

Fig. 2. Cap model yield surfaces.

$$f_1(\sigma) = T - J_1 = 0 \tag{5}$$

$$f_2(\sigma) = s - F_e(J_1) = 0 \quad \text{for} \quad -T \leqslant J_1 \leqslant L(k) \tag{6}$$

where

$$F_e(J_1) = \alpha - \gamma e^{-\beta J_1} + \theta J_1 \tag{7}$$

and

$$L(k) = \begin{cases} k & \text{if } k \succ 0 \\ 0 & \text{if } k \leqslant 0 \end{cases} \tag{8}$$

In these equations, T is the tension limit, k is the internal state variable that represents the material hardening whereas α, β, γ and θ are additional material parameters all to be determined experimentally and characterizing the shear failure behavior.

On the other hand, the yield surface that represents the densification of the metal powder aggregate is chosen to be an elliptical cap normal to the isostatic stress axis J_1. This surface can be represented by the function given in (Eqs. (9) and (10)) where R is the cap aspect ratio usually assumed constant and $X(k)$ is the intersection of the cap surface with the J_1 axis

$$f_3(\sigma, k) = F_c(J_1, s, k) - F_e(k) = 0 \quad \text{for} \quad L(k) \leqslant J_1 \leqslant X(k) \tag{9}$$

$$F_c(J_1, s, k) = \sqrt{s^2 - \frac{1}{R^2}[J_1 - L(k)]^2} \tag{10}$$

This cap formulation proposed by Hofstetter et al. (1993) is somewhat different from the classical one proposed by Dimaggio and Sandler (1971) and Simo et al. (1988), and offers better algorithmic robustness. It has also been proposed that the aspect ratio R of the cap should be an increasing function of density so as to better represent ductile powder compaction behavior (Trasorras et al., 1989):

$$R(\rho) = \frac{(X(k) - k)}{F_e(k)} \tag{11}$$

Moreover, an associative flow rule was adopted. No experimental observations did in fact justify the use of a more complicated non-associative flow rule. This rule, appropriate for multi yield surface plasticity, is defined in (Eq. (12)), where $\dot{\lambda}_i$ is the plastic consistency parameter associated with the yield surface function f_i.

$$\dot{\varepsilon}^p = \sum_{i=1,3} \dot{\lambda}_i \frac{\partial f_i(\sigma, k)}{\partial \sigma} \tag{12}$$

The numerical implementation of the constitutive equations presented here requires special care especially when dealing with the singular corners resulting from the non-smooth intersection of the yield surfaces.

2.3.3. Hardening law

The hardening of the cap surface is modeled through the evolution of the state variable k. This evolution is given by the rule relating k to the effective volumetric plastic strain $\bar{\varepsilon}_v^p$ in a form suggested by the results of the classical isostatic pressing test (Eq. (13)).

$$\bar{\varepsilon}_v^p[X(k)] = W[1 - e^{-DX(k)}] \tag{13}$$

In the equation above, W and D are two material parameters and $\bar{\varepsilon}_v^p$ is the effective volumetric plastic strain expressed in terms of stress first invariant $X(k)$ and defined in a manner that prevents the cap strain softening (Dimaggio and Sandler, 1971):

$$\bar{\varepsilon}_v^p = \begin{cases} \varepsilon_v^p & \text{if } \varepsilon_v^p \text{ or if } (k > 0 \text{ and } k > J_1) \\ 0 & \text{otherwise} \end{cases} \tag{14}$$

The volumetric plastic strain ε_v^p is the trace of the plastic strain tensor ε^p. This quantity is used to update the actual aggregate density ρ using the initial loose state density ρ_0 as follows:

$$\rho = \rho_0 e^{-\varepsilon_v^p} \tag{15}$$

3. Experimental characterization of the cap material model

3.1. Overview

The calibration task is usually performed through numerical trial and error process without following a clear methodology. A mathematical approach was followed by Simo et al. (1988) who considered the task of parameter identification from experimental results as an optimization problem and solved it using the Marquardt–Levenberg algorithm.

In this research, an experimental characterization methodology is developed for the cap model. It was applied for a blend of Alcan 316L stainless steel powder with 0.75 wt.% premixed Acrawax lubricant. The blend had a loose relative [1] density of 0.33 (2.64 g/cm^3), and its particle size distribution is given as follows in term of mesh size and associated relative distribution level: [+80 mesh (0%); −80/+100 mesh (0.01%); −100/+150 mesh (2.6%); −150/+200 mesh (11.2%); −200/+325 mesh (31.9%); −325 mesh (54.3%)].

First, the powder medium elastic moduli were determined from resonant frequency measurements. Then, a series of isostatic compression tests were carried out to determine the parameters of the model hardening law. The same tests, together with additional triaxial and uniaxial compression tests were used to determine the parameters of the cap and of the shear failure surfaces. Finally, considering that tensile loading is irrelevant for rigid die compaction modeling, the tension limit was supposed to be equal to zero (Fig. 3).

The first step of the experimental procedure was to isostatically press specimens at different pressures ranging from 20 to 90 ksi (138 to 610 Mpa). Isostatic compression was preferred over other processes since it generates parts with quasi-constant densities. Then, specimens were machined into bars having an appropriate shape for the remaining tests. A detailed description of the equipment used in this research is

[1] The ratio of porous medium density to the corresponding wrought material density.

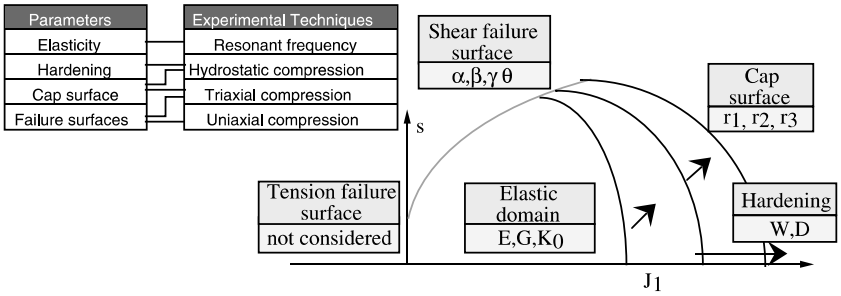

Fig. 3. Cap model parameters and associated experimental measuring techniques.

presented in Gurson and Posteraro (1992) and Yu et al. (1992). The obtained set of parameters was then validated by way of FE simulations aimed at reproducing the results of the calibration tests.

3.2. Elastic parameters

Resonant frequency measurements (Yu et al., 1992) were taken on rectangular bars of dimensions: 1.25 in. × 0.5 in. × 0.25 in. and with densities ranging from 71% to 84%. No bars with lower densities could be tested due to machinability limit of the material. Using the appropriate relations (Spinner and Tefft, 1961), Young (E) and Shear (G) moduli were determined as functions of the compact density, within an accuracy of respectively 4% and 2%. Fig. 4 shows the obtained results together with the fitted relations and the corresponding correlation factors R. The bulk modulus K was then derived from the E and G functions.

It is important to note that the extremely small values of elastic parameters, especially in the low density range, could not be interpreted simply as high "elastic softness". Hence, the values obtained for green compacts could not be interpreted as those obtained for wrought materials. In fact, it is known that no elasticity is present in the first stages of the compaction of loose metal powders, whereas high density compacts behave elastically in a way that is similar to wrought materials (Alm, 1983). However, the density threshold at which the measured values could be considered as "conventional" elastic parameters is not yet determined. This could be done by way of loading/unloading cycles in an instrumented isostatic press. However, since the cylindrical fluid type press used in this research was not fully instrumented, it did not permit this kind of testing. Currently, in order to overcome this limitation, a fully instrumented

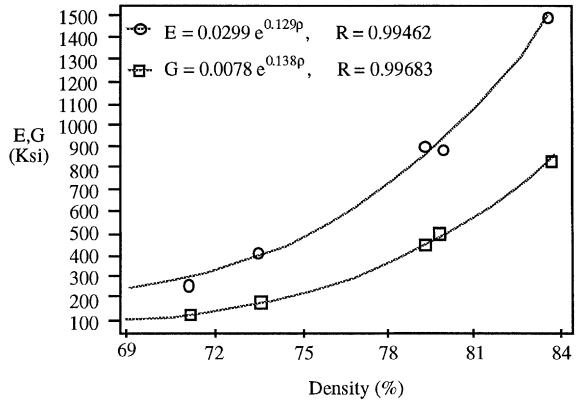

Fig. 4. Young and shear moduli as functions of relative density.

experimental press is under development in our laboratory. A better characterization of the elastic behavior, in terms of stress as a function of recoverable strain, is thus foreseen.

Accordingly, for the simulations included in this work, the elastic parameters will be considered as constants. Their values will be determined by using equations of Fig. 4 with a density corresponding to the average final density of the compact.

3.3. Hardening law

The hardening law is the model component that describes the compressibility of the studied powder. It corresponds to the relation between the plastic volumetric strain ε_v^p and the stress tensor first invariant J_1. Ideally, this could be obtained from an isostatic compression of a loose powder specimen in an instrumented isostatic chamber. However, since the available pressure chamber was not instrumented, we had to perform several tests with different set pressures. For each test, the plastic volumetric strain was computed from the powder initial density ρ_i and the final compact density ρ_f (Eq. (16)). These two densities were measured by the procedures described respectively in MPIF standards (MPIF, 1986, 1992).

$$\varepsilon_v^p = \ln \frac{\rho_f}{\rho_i} \tag{16}$$

The obtained values were plotted against the first stress invariant corresponding to the isostatic set pressure (Fig. 5). Then, data were fitted to the general form of the hardening law (Eq. (17)). The fitting process permitted the determination of two important cap model parameters: $W = 91.64\%$ and $D = 1.97 \times 10^{-3}$ ksi^{-1}, W being a measure of the maximum achievable volumetric plastic strain.

$$\varepsilon_v^p = W(1 - e^{-DJ_1}) \tag{17}$$

3.4. Yield functions

Given that our primary objective is to model the compaction stage of the forming process, we have mainly focused our attention on determining the cap yield surface rather than the two other failure surfaces. Assuming that such a surface is the collection of all the yield stress states of an aggregate having a certain relative density (Chtourou et al., 1995), we had to probe the J_1–s stress space to determine the cap surface for a certain number of relative densities. This was achieved by carrying out a series of triaxial compression tests. During these tests, the powder specimens, encapsulated into a triaxial fixture consisting of two

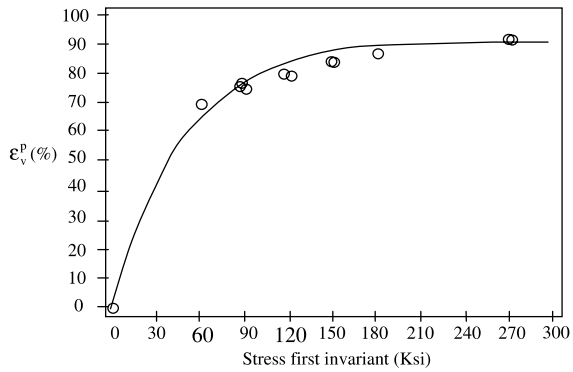

Fig. 5. Hardening law fitting from isostatic test results.

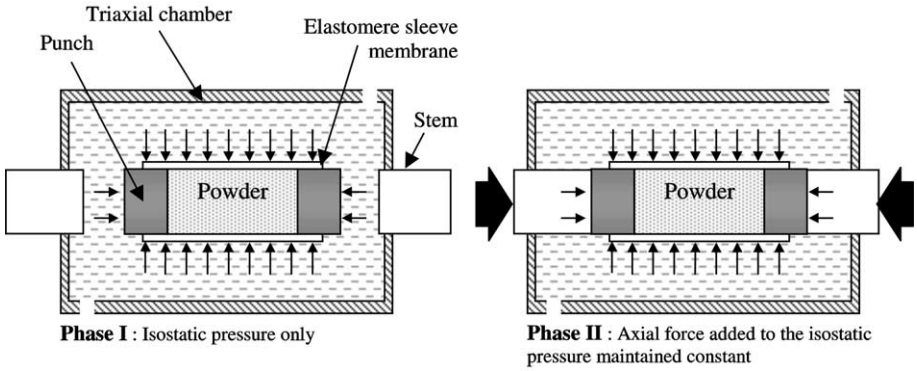

Fig. 6. Triaxial compaction test.

punches and an elastomer sleeve, were first subjected to a isostatic fluid pressure. When the set pressure was reached, additional axial force was mechanically applied to the specimens while the machine control system maintains the fluid set pressure constant (Fig. 6). The axial load was slowly increased until fracture of the specimen was reached. During these tests, sticking contact was assumed between the powder and the punches.

The data acquisition system of the apparatus was used to obtain on line measurements of the volumetric and axial strains, fluid pressure and axial force (Innovare, 1993). However, since loose powder undergoes a large portion of its total deformation in the early stages of the test, the shape of the elastomer rapidly becomes inadequate and the measured data loose accuracy. Thus, the tests were performed on isostatically pre-pressed [2] cylindrical slugs having a diameter of 0.625 in. and a length of 1.38 in. (Gurson and Posteraro, 1992).

Furthermore, a special purpose program was used for filtering and for processing the collected data in order to determine values of some useful variables, such as the equivalent deviatoric stress, the total isostatic stress and the actual compact density. Moreover, in spite of the specimen slightly barreled shape, obtained following its removal from the triaxial fixture, we assumed, for volume and density calculation purposes, that it remains cylindrical throughout the whole load path. Fig. 7 shows the load paths of some of the performed triaxial tests. The first two digits in a load path label refer to the value in ksi of the pre-compaction isostatic pressure whereas the last two digits designate the isostatic set pressure of the actual triaxial test.

Using the collected volumetric deformation and knowing the initial density of the tested specimen, we could monitor the evolution of density as shown in Fig. 8. It should be noted that the only strains taken into account to update the density are those measured after reaching a isostatic pressure equal to the pre-compaction pressure. In fact, strains measured before this level were assumed to be totally elastic. During experimental testing, additional load paths at higher isostatic set pressure were carried but their results were not useable due to the occurrence of high noise level in the measurements. In fact, the triaxial machine started showing instability at isostatic pressures as high as 60 ksi. This is not however a major handicap for the cap model fitting process since the exploitable tests (3030, 4040 and 5050) covered the usually attainable stress levels as encountered in practical rigid die compaction situations.

[2] The pre-compaction hydrostatic pressure is always equal or lower than the hydrostatic set pressure of the triaxial test in order to obtain a quasi-monotone global load path.

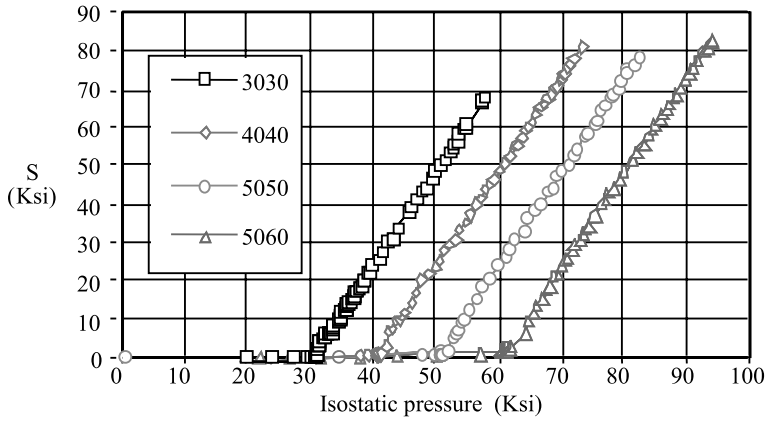

Fig. 7. Load paths of four triaxial tests.

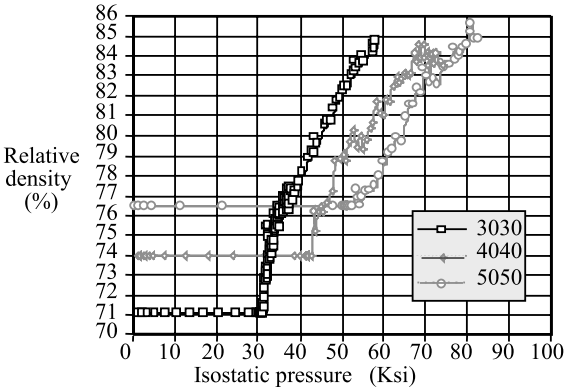

Fig. 8. Density evolution during triaxial tests.

In other respects, it may be seen from Figs. 8 and 9 that none of the load paths led to a shear failure occurrence. In fact, the axial load applied by the apparatus was not sufficient to reach such critical states in which the densification of specimens reaches a maximum value and above which they can experience volumetric dilatancy followed by fracture (Chtourou et al., 1995). Hence, for the determination of the shear failure surface, we used only data points given by the free uniaxial compression (Fig. 9). This brings down the failure surface to a straight line in the J_1–s stress space. Therefore, further tests are required in order to obtain a more reliable shear failure surface.

3.5. Analysis of the model sensitivity

A sensitivity study of the model showed that the lack of information concerning the shear failure surface, as well as the lack of accuracy of the apparatus, does not represent a major handicap to the entire characterization procedure, when the final green density is the main concern. In fact, a study based on simulations planned and analyzed using the Taguchi method (Chtourou, 1996) where material parameters were considered as "control factors" was carried out. This study revealed that, when dealing with powder compaction with no excessive distortion, the parameters that most affect the final density distribution are

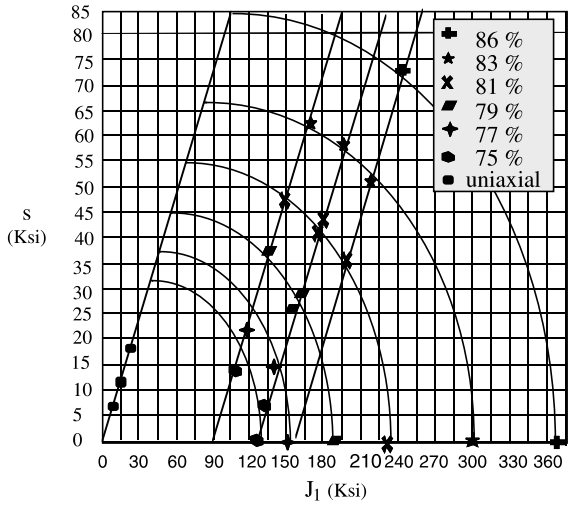

Fig. 9. Fitting of the cap surfaces and the shear failure surface.

those related to the material hardening law. The range of variation for all the parameters was taken as ±5% around the set value except for parameter K_0 and for the shear failure parameters which had null set values. For these last parameters, larger variation ranges were required in order to obtain a significant perturbation of the model results (Ross, 1988). All these simulations were concerned with a simple cylindrical slug subjected to rigid die compaction with ideal frictionless die contact.

Table 1 summarizes the preliminary model parameter values obtained for the 316L stainless steel powder, as well as their respective relative influence on the final density distribution in a compact, as determined by the sensitivity analysis. It should be noted that the cap initial position was not determined experimentally but was simply taken as a very small value, implying that the powder had no elastic behavior when in the loose state.

3.6. Validation of the material parameter set

A series of FE simulations were carried out in order to validate the material parameters. These simulations are aimed at reproducing the experimental tests, namely the isostatic and the triaxial compaction tests, used to calibrate the model. The simulations were based on a single axisymmetric element mesh,

Table 1
Values and relative influence of the 316L parameters

Parameters	Units	Values	Relative influence (%)
E	ksi	Function (Fig. 4)	19.32
G	ksi	Function (Fig. 4)	11.29
α	ksi	0	0.83
β	ksi^{-1}	0	0.06
γ	ksi	0	0.68
θ	–	0.617	0.32
W	–	0.916	54.47
D	ksi^{-1}	0.00197	12.21
R	–	Function (Eq. (18))	0.64
K_0	ksi	0.001	0.01

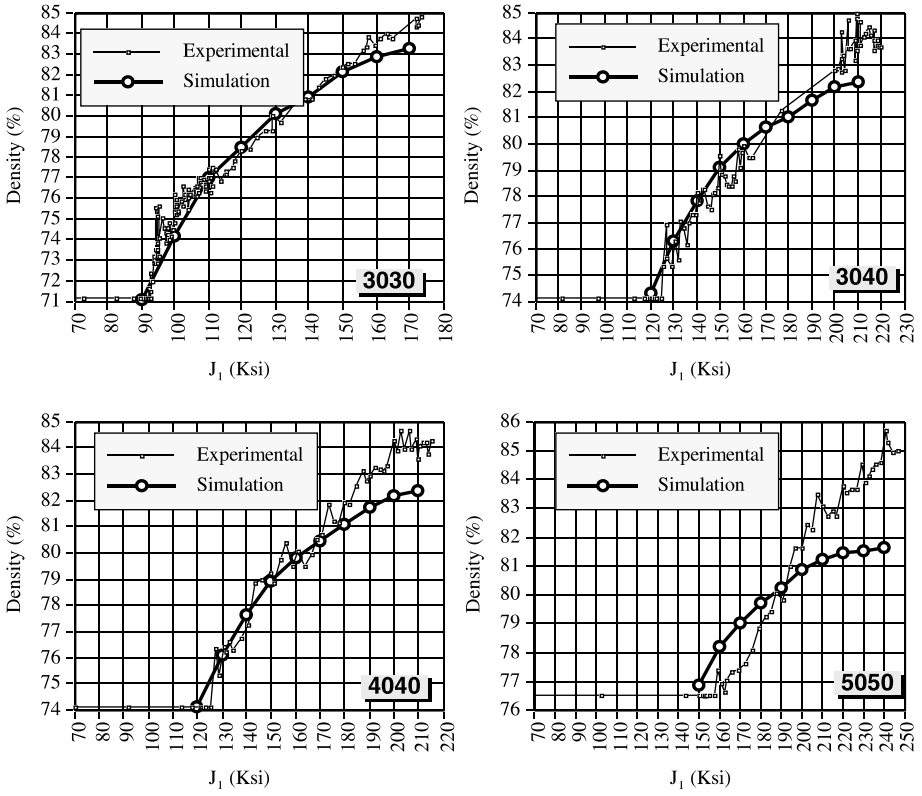

Fig. 10. Simulation results of the triaxial compression tests.

subjected to imposed pressures corresponding to experimental conditions. The results of the two series of simulation are graphically shown, in terms of achieved relative density, in Figs. 10 and 11.

As shown in these figures, a good agreement between experimental and simulated results was achieved for most cases. In fact, except for the 5050 triaxial compaction test, discrepancy never exceeded 1.5% (in

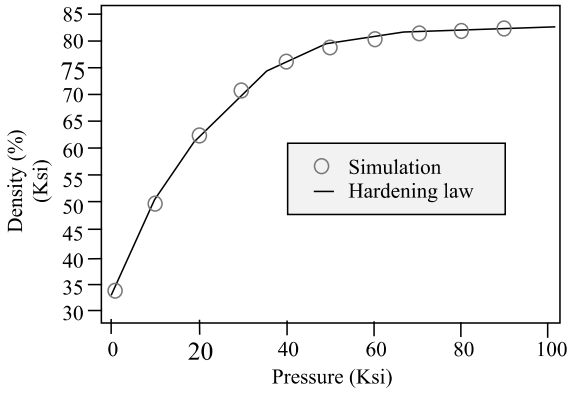

Fig. 11. Simulation results of the isostatic compression tests.

terms of relative density). The higher discrepancy that appears only at the late stages of compression is due to an approximation used in processing the triaxial tests data and hence does not result from an eventual inaccuracy of the model. In fact, as mentioned earlier, it was assumed, for a preliminary data analysis, that once the pre-compaction pressure is reached, all subsequent deformation is totally plastic. However, it appears that accumulated elastic strain, which should not be accounted for in density calculation, is not as small as we assumed, but can reach as much as 3%. This explains why the experimental density is as much as higher than the predicted one.

Globally, the results obtained from the model are largely acceptable, knowing that the experimental tests involved considerable noise (Ross, 1988). Accordingly, the obtained values for the material parameters are considered to be valid and are retained for the rest of simulations.

4. Experimental validation technique

4.1. Overview

Different techniques for local density evaluation have been developed and proposed for the last twenty years. Generally, these techniques were compared to bulk density measurements (e.g. wet/dry technique) taken on part samples of supposedly constant density. Unfortunately, most if not all of these local density evaluation techniques are still under development for reason of considerable measurement variability that is caused in turn by inadequate control of sample preparation and testing.

Because local density can be correlated to part conductivity, hardness and several other more easily measured properties, indirect techniques have grown in popularity. In a previous research (Guillot et al., 1995), we reviewed the most commonly used methods. We also established the sensitivity of factors involved during sample preparation and testing, attempted to improve the technique and assessed the accuracy, for two promising local density evaluation techniques: (1) Vickers hardness and (2) analysis of images obtained using an optical microscope. Even though excellent results were obtained with both techniques, the first is chosen in practical applications due to its less demanding experimental protocol. The basic elements of this protocol are presented in the remaining part of this section.

4.2. Sample preparation

Samples of 2 cm diameter by 0.7 cm height were compacted into a billet shape. Pressing ranging between 20 and 60 tsi (tons per square inch) provided billets of different density levels. The green compacts were lightly sintered to remove the lubricant and to improve strength for sectioning and metallographic sample preparation. However, it was important to avoid the alteration of their densities. Consequently, each billet was sintered in 100% H_2 atmosphere for 30 min at 450 °C temperature. Then, density was determined as the weight divided by the volume as measured with a micrometer.

In addition, the billets were cut using a diamond wheel and both cut sections were mounted in a Lucite mounting cup. Afterwards, samples were ground and polished on a versatile grinder-polisher with room for six samples and rotating at 30 rpm, following the conditions of Table 2.

4.3. Vickers hardness measurements and correlation with density

This Vickers hardness measurement technique was used to obtain apparent hardness also called macro-hardness, i.e. the average hardness of a porous material. Its procedure is well documented in ASTM E92-82 standard (ASTM, 1987). This standard offers various loading from 1–120 kgf applied to an indenter of pyramidal geometry with face angle of 136°. In this work, a 5 kgf load (HV 5) was used as recommended in

Table 2
Polishing conditions

	Grinding	Polishing		
		Rough	Medium	Fine
Material	180 grit	320 grit	600 grit	5 μ alumine
Passing weight	1 lb	1 lb	1 lb	1 lb
Time	Until surface flat and without defect	1.5 min	1.5 min	2.0 min

Table 3
Correlation between density and Vickers hardness

Experiment	Billet green density (%)	Vickers hardness HV (kg/mm^2)			
		Average		Standard deviation	
		Face A	Face B	Face A	Face B
1	77.9	44.3	46.2	2.58	2.22
2	80.3	54.6	54.3	4.38	2.26
3	82.0	61.8	62.6	2.69	2.18
4	84.2	71.1	71.7	4.23	1.92
5	86.3	81.5	81.5	2.64	2.64

MPIF standard 43 (MPIF, 1991). Measurements were performed on five billets of different densities. Each billet had two faces on which $n = 15$ hardness measurements were realized in a 3×5 pattern. The results are reported in Table 3.

As shown in Fig. 12, the relationship between the green density and the logarithm of Vickers hardness can be correlated with a linear model. Using a linear regression technique, the density of green compacts (GC) becomes:

$$\text{Density } (\%) = \rho_{\text{HV,GC}} = 32.72 \ \log(\text{HV}) + 23.56 \tag{18}$$

Error limits introduced by this model, by sample preparation factors and by the hardness measurements can be established to $\pm(0.05 + 7.8/n)^{1/2}$ with a confidence level of 68%. Curiously, most of the error is caused by the Vickers measurement, and thus, can significantly be reduced by taking and averaging "n" measurements in a small area.

Thus, to obtain the local density distribution in any compact made of the studied powder, this part should first be prepared following the presented experimental protocol. Then, Vickers hardness measure-

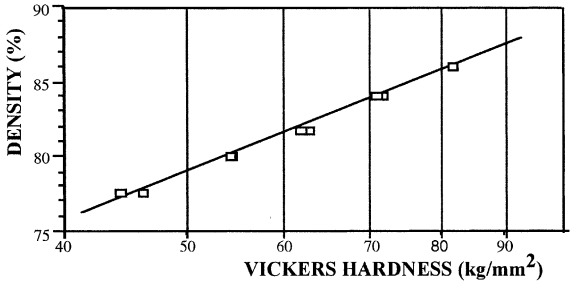

Fig. 12. Linear relationship between density and Vickers hardness.

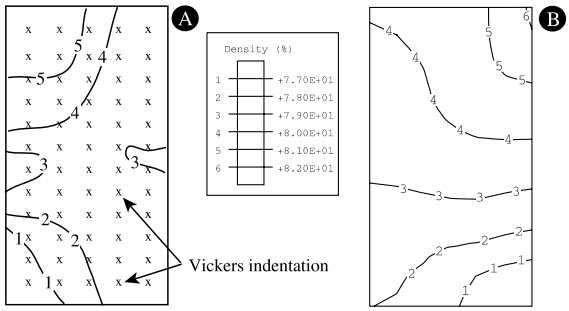

Fig. 13. (A) Experimental vs (B) simulation results.

ment could be taken and translated into density measurements using the established calibration curve. Finally, it was proved that this technique could be applied with a similar accuracy to other powder materials (Guillot and Chtourou, 1996).

5. Application

A simple cylindrical part made of 316L stainless steel powder was pressed on an a 50 ton mechanical press. The tooling needed to press this part consisted of a die, a lower punch and an upper punch. An axisymmetric model of this application was used to determine the final density distribution in the compact.

Besides, an integrated simulation module, designed so as to render the modeling approach practical and industrially usable, was developed. This module permits an easy definition of the tooling and the powder geometry, as well as the compaction sequence and all other boundary conditions. It also handles FE solution and results post processing. [3] The density distribution obtained after the three step compaction sequence compares well to the experimental density map (Fig. 13). This map was obtained by the way of a specially developed method based on the correlation of local density and Vickers macro-hardness.

6. Conclusion

This paper addressed the material characterization and validation of a particular cap model originally developed to deal with geological materials and properly adapted so as to handle ductile metal powders. An experimental characterization procedure has been developed and applied for the case of 316L stainless steel powder. The obtained material parameter set was validated by way of the simulation of the characterization tests and served as a basis for the model parameters sensitivity analysis. This study proved that the imperfections of the procedure do not affect the most influent parameters.

In addition, an experimental technique for the evaluation of the local density distribution was developed in order to validate the simulation results. This technique, based on a correlation with Vickers macrohardness measurements, permits an accuracy of 1% in terms of relative density. An integrated simulation module, developed in a related research was also used to run a simulation of the compaction of an industrial PM part. The comparison of the obtained density distribution with an experimentally measured map served as a validation for the modeling approach.

[3] Through the software Abaqus and Abaqus-Post respectively.

Presently, our main research orientations are the improvement of the model characterization procedure to include a better description of the powder elastic behavior. Furthermore, 3D simulation module, capable of modeling general non-axisymmetric applications, is under development.

Acknowledgements

The authors would like to thank Mr. Sébastien Parent and Ms. Isabelle Jacob from Précitech Inc. for the experimental assistance as well as M. Christian Michaud, Mrs. Cathryn Macrander and M. André Hengartner for their help in software development. The authors would also like to acknowledge the support of the National Sciences and Engineering Research council of Canada (strategic grant nos. 0167091 and CRD-186296).

References

Alm, O., 1983. Mechanical testing of powders and powder compacts. Scandinavian Journal of Metallurgy 12, 302–311.

ASTM, 1987. Standard E92-82, Standard Test Method for Vickers Hardness of Metallic Materials.

Biba, N.V., Keife, H., Sthalberg, U., 1993. A finite element simulation of powder compaction confirmed by model-material experiment. Journal of Materials Processing Technology 36, 141–155.

Brown, S., Abou-Chedid, G., 1993. Evaluation of yield functions due to powder characteristics. Advances in Powder Metallurgy and Particulate Materials 3, 245–255.

Chtourou, H., 1996. Modélisation par Éléments Finis du Procédé de Compression des Poudres Métalliques de l'Acier Inoxydable 316-L. Ph.D. Thesis, Laval University, Quebec.

Chtourou, H., Guillot, M., Gakwaya, A., 1995. Modeling the rigid die compaction of 316L stainless steel powder. Advances in Powder Metallurgy and Particular Materials 1 (2), 169–183.

Crawford, J., Lindskog, P., 1983. Constitutive equations and their role in the modeling of the cold pressing process. Scandinavian Journal of Metallurgy 12, 271–281.

Dimaggio, F., Sandler, I., 1971. Material model for granular soils. Journal of the Engineering Mechanics Division, 935–950.

Doraivelu, S.M., Gegel, H.L, Gunasekera, J.S, Malas, J.C., Morgan, J.T., Thomas, J.F., 1984. A new yield function for compressible P/M materials. International Journal of Mechanical Sciences 26, 527–535.

German, R.M., 1984. Powder Metallurgy Science. MPIF, Princeton, NJ.

Guillot, M., Chtourou, H., 1996. Generalization of the Vickers hardness local density measurement technique to different powder materials, Proceedings of the World Congress on Powder Metallurgy and Particulate Materials, vol. 1, part 4, Washington DC, pp. 31–40.

Guillot, M., Chtourou, H., Parent, S., 1995. Modeling the rigid die compaction of 316L stainless steel powder. Advances in Powder Metallurgy and Particular Materials 3 (9), 31–49.

Gurson, A.L., Posteraro, R.A., 1992. Yield functions for metal powders for use in the numerical simulation of powder compaction, TMS Conference, San Diego CA.

Hofstetter, G., Simo, J.C., Taylor, R.L., 1993. A modified Cap model: closest point solution algorithms. Computers and Structures 46 (2), 203–214.

Innovare Inc. 1993. Advanced Metalworking System, Bath, PA, vol. 114, no. 2.

Jagota, J., Dawson, P.R., 1988a. Micromechanical modeling of powder compacts-I. Unit problems for sintering and traction induced deformation. Acta Metallurgica 36 (9), 2551–2561.

Jagota, J., Dawson, P.R., 1988b. Micromechanical modeling of powder compacts-II. Truss formulation of discrete packing. Acta Metallurgica 36 (9), 2563–2573.

Koopman, M.G., Rachakonda, V.B.S., Gurson, A.L., McCabe, T., 1992. Material models for the finite element simulation of compaction of metal powder, TMS Fall Meeting, Chicago.

Kuhn, A.H., Downey, C.L., 1971. Deformation characteristics and plasticity theory for sintered powder materials. International Journal of Powder Metallurgy 7 (1), 15–25.

Lenel, F.V., 1980. Powder Metallurgy, Principles and Applications. MPIF, Princeton, NJ.

MPIF, Standard 04, 1992. Using the Hall Apparatus, Determination of Apparent Density of free Flowing Metal Powders, Princeton, NJ.

MPIF, Standard 42, 1986. Determination of Density of Compacted and Sintered Metal Powder Products, Princeton, NJ.

MPIF, Standard 43, 1991. Method for Determination of Hardness of Powder Metallurgy Products.
Ross, P.J., 1988. Taguchi Techniques for Quality Engineering. McGraw-Hill, New York.
Sandler, I.S., Rubin, D., 1979. An algorithm and a modular subroutine for the Cap model. International Journal for Numerical and Analytical Methods in Geomechanics 3, 173–186.
Shima, S., Oyane, M., 1976. Plasticity theory for porous material. International Journal of Mechanical Science 18, 285–291.
Shima, S., Saleh, M.A.E., 1993. Variation of density distribution in compacts in closed die compaction with powder characteristics. Advances in Powder Metallurgy and Particulate Materials 3, 175–189.
Simo, J.C., Ju, J.W., Pister, K.S., Taylor, R.L., 1988. Assessment of Cap model: consistent return algorithms and rate dependent extension. ASCE Journal of Engineering Materials 114 (2), 191–218.
Spinner, S., Tefft, W.E., 1961. ASTM proceedings, Engineering, p. 1221.
Trasorras, J., Krauss, T.M., Fergusson, B.L., 1989. Modeling the powder compaction using the finite element method, Proceedings of the 1989 International Conference on Powder Metallurgy, San Diego, CA, pp. 85–104.
Weber, G.G., Brown, S.B., 1989. Simulation of the compaction of powder components. Advances in Powder Metallurgy and Particulate Materials 1, 105–118.
Yu, C.J., Henry, R.J., Prucher, T., Parthasarathi, S., Jo J., 1992. Reasonant frequency measurements for the determination of elastic properties of P/M components, Proceedings of the P/M'92 World Congress, vol. 6, pp. 319–332.